

Pyroelectricity of Lead Sulfide (PbS) Quantum Dot Films Induced by Janus-Ligand Shells

Zhiyuan Huang, Ji Hao, Jeffrey L. Blackburn, and Matthew C. Beard*



Cite This: <https://doi.org/10.1021/acsnano.1c05185>



Read Online

ACCESS |



Metrics & More



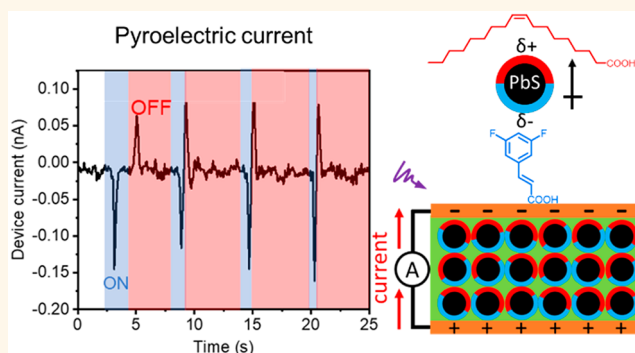
Article Recommendations



Supporting Information

ABSTRACT: Asymmetry is an essential property to control. To do that in nanocrystalline systems we have developed methods to produce Janus-ligand shells on otherwise symmetric PbS quantum dots (QDs). Here, we demonstrate that control by constructing a system that exhibits pyroelectricity built from spherical PbS QDs. We observed a pyroelectric current in two different configurations. In one configuration, the QDs are self-assembled into close-packed arrays while in the second configuration, the QDs are dispersed into an electro-inactive polymer, polydimethylsiloxane. Both exhibit a pyroelectric response. In the first configuration we estimate a lower limit of the pyroelectric coefficient to be $1.97 \times 10^{-7} \text{ C/m}^2\text{K}$, which is likely limited by the degree of QD alignment during film formation but is already on par with common pyroelectric systems. Compared with inorganic ceramic-like and polymeric pyroelectric materials, pyroelectric films self-assembled from polar QDs are easier to prepare, responsive to light with different energies based on QD exciton energy, and the polarization of each QD could be easily tuned by constructing different Janus-ligand shells.

KEYWORDS: pyroelectricity, quantum dots, Janus, lead sulfide, asymmetric ligand shell



INTRODUCTION

The most important component of any electroactive system is an asymmetry in the fundamental building blocks that when aligned leads to a macroscopic polarization. In fact, all energy converting systems have some form of asymmetry at the molecular or systems level that must be introduced. In this work, we introduce a proof-of-concept method to construct an artificial pyroelectric system that exhibits spontaneous electrical polarization and, thus, demonstrate the concept for constructing a larger class of electroactive systems. Energy harvesting is a topic that draws the attention of many researchers due to growing energy demand, a large need for carbon-free energy sources, and the need to enhance energy utilization. Specifically, the topic of harvesting thermal energy is attractive to both academic and industrial researchers. It has been reported that more than half of the energy consumed in the United States is wasted as low-grade heat.¹ Thermoelectricity and pyroelectricity are two strategies that are able to transform thermal energy to usable electrical energy. Specifically, thermoelectricity^{2,3} operates according to the Seebeck effect to generate electrical power from a temperature gradient. Such a system requires heat sinks to maintain the temperature gradient. In contrast, the pyroelectric effect^{4,5} generates electricity from temperature fluctuations, without the

need for a heat sink. In the pyroelectric effect, electricity is generated due to a change in polarization, similar to piezoelectricity. For piezoelectricity, the change in polarization occurs from mechanical stress, while for pyroelectricity it occurs from a temperature change. All pyroelectric materials are also piezoelectric.

For the pyroelectric effect, the key component is spontaneous electrical polarization. The desired polarization is built-up differently in different pyroelectric systems.⁵ However, most pyroelectric systems consist of inorganic ceramic-like, single or polycrystalline, e.g. triglycine sulfide,^{6,7} lead magnesium niobate,⁸ strontium barium niobate,⁹ zinc oxide,^{10,11} etc. The polarization within these systems is determined by the underlying polar crystal structure and below a critical temperature domains align to form a macroscopic polarization. Though large pyroelectric coefficients are observed, the high stiffness and brittleness of these

Received: June 17, 2021

Accepted: August 13, 2021

systems limit their use in flexible electronic applications. To overcome this limit, polymeric pyroelectric materials such as poly(vinylidene fluoride) (PVDF) or poly(3,4-ethylenedioxythiophene)s (PEDOTs)¹² and related derivatives have been developed.^{6,13,14} Three phases exist for basic PVDFs due to the conformation of the polymer chain, and efforts must be made to transform the electro-inactive, but most thermodynamically stable, α phase to an electroactive phase, i.e., the β and γ phases.^{15–17}

Here we introduce a way to construct a pyroelectric system from nominally nonpyroelectric building blocks using the techniques of nanochemistry and taking advantage of the inorganic/organic nature of nanocrystals, specifically, organic ligands attached to the surface of inorganic semiconductor nanocrystals, or quantum dots (QDs), that help to define and determine their physicochemical properties. Here, pyroelectric thin films were prepared with spherically symmetric PbS QDs that have an asymmetric ligand shell (so-called Janus-ligand shell). The spontaneous polarization arises from the asymmetric Janus-ligand shell which renders a dipole moment to the symmetric QD building blocks, while the spherical and colloidal nature of the QDs allows for close packing in films and arrays. The asymmetric ligand shell here includes nonpolar oleic acid (OA) molecules, and electron-withdrawing 3,5-difluorocinnamic acid (CAH) molecules (Figure 1). We select

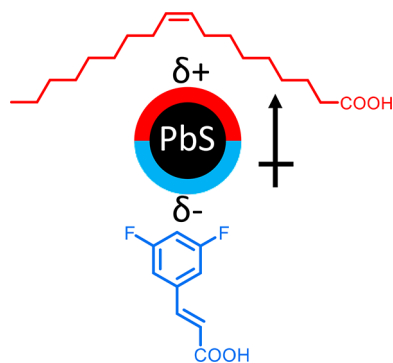


Figure 1. Janus-ligand shells on PbS QDs form the building block of pyroelectric films.

3,5-difluorocinnamic acid, from a number of potential derivatives, since the formation of a Janus-ligand shell has been confirmed by 2D nuclear magnetic resonance spectroscopy.¹⁸ The electron withdrawing effect of the CAH polarizes the PbS QDs, which are then self-assembled into films under an electric field where the polarization direction of each QD aligns with the direction of the electric field. Once assembled the electric field is removed but the macroscopic polarization remains.

RESULTS AND DISCUSSION

PbS QDs with Janus-Ligand Shells. To demonstrate the pyroelectric concept of Janus-ligand shells, we start with PbS QDs that have a first exciton absorption peak at 1050 nm corresponding to QDs with an average diameter of 3.5 nm (Figure 2a, see the Materials and Methods section for synthetic details). PbS QDs are good light absorbers with high absorptivity. Additionally, the small bandgap of PbS QDs, combined with high energy excitation, guarantees that enough excess energy could be converted to heat through exciton thermalization. But, in principle, the approach demonstrated

here should be applicable to other nanoscale systems where the asymmetry of the building blocks arises from the Janus-ligand shells. To find the conditions that yield a Janus-ligand shell we use spectrophotometric titrations (Figure 2). The exchange of the nonpolar oleate ligand with a conjugated polar ligand on PbS QDs results in broad enhancement of the QD absorbance, which has been observed with many conjugated ligands.^{19–21} Figure 2a presents the absorption of PbS QDs after ligand exchange reaction with varying concentrations of 3,5-difluorocinnamic acid (CAH). The absorptivity increases as the CAH/PbS ratio increases. We also observed a red-shift of the first exciton peak as CAH binds to the PbS QDs (Figure 2a inset), which is attributed to exciton delocalization onto the CAH ligands.¹⁹ Because the absorption feature of the CAH molecules occurs to the blue of 400 nm, the area under the curve from 400 to 1200 nm is integrated to determine the absorbance enhancement. There is a square-root correlation between the QD absorbance enhancement and the number of bound CAH ligands.²¹ As such $(\Delta\alpha/\alpha_0)^2$ reflects the number of bound ligands, where $\Delta\alpha$ is the enhanced absorbance of PbS/CAH QDs compared to PbS/OA QDs, and α_0 is the absorption of PbS/OA QD.

Thus, the plot of $(\Delta\alpha/\alpha_0)^2$ vs CAH/PbS equivalents represents the adsorption isotherm of the ligand exchange reaction and reaches a maximum when the CAH/PbS ratio equals to 500 representing the condition of full ligand exchange. The steep rise of the isotherm near CAH ligand equivalents of 100 (dashed line in Figure 2b) indicates that the system undergoes a sharp transition from all oleate bound ligands to all cinnamate bound ligands. Such a sharp transition indicates the ligand exchange reaction is highly cooperative such that bound cinnamates prefer to be surrounded by other bound cinnamates. Such behavior was recently studied in depth using a modified two-dimensional (2D) lattice model that includes a ligand–ligand coupling parameter to capture the ligand cooperative exchange.¹⁸ For ligands with high cooperativity the results suggest that the ligand shell in the transition region becomes Janus-like. The black trace in Figure 2b is the best-fit of the 2D-lattice model to our data. The best-fit ligand–ligand coupling parameter, ΔJ , was $-0.48k_B T$ which indicates that the ligands tend to segregate on the QD surface during the ligand exchange reaction. We use that result here to construct our asymmetric QD building blocks that make up the pyroelectric demonstration. It is worth noting that the absorption enhancement decreases when CAH/PbS ratio reaches 1000. This we hypothesize is because the π – π stacking between CAH ligands decreases the PbS–CAH electronic interaction that induces absorption enhancement. The drop of absorption enhancement with CAH was not observed in our previous study due to different sizes of PbS QDs and the higher QD concentration used here. In this study, we choose the CAH/PbS ratio of 100 as the ligand exchange condition to construct PbS QDs and corresponds to a surface coverage of $\sim 35\%$. This is because higher coverage may lead to less of an overall dipole moment.

2D Nuclear Magnetic Resonance (NMR) spectroscopy confirms the formation of patchy ligand shells. Figure 3. shows the 2D nuclear Overhauser effect spectroscopy (NOESY) of PbS QDs after ligand exchange with CAH ligands. NOESY characterizes the through-space ligand–ligand interaction on PbS QD surfaces. Strong cross-peaks should be observed when OA and CAH ligands are within ~ 0.4 nm of one another and thus, when observed, correspond to a randomly distributed

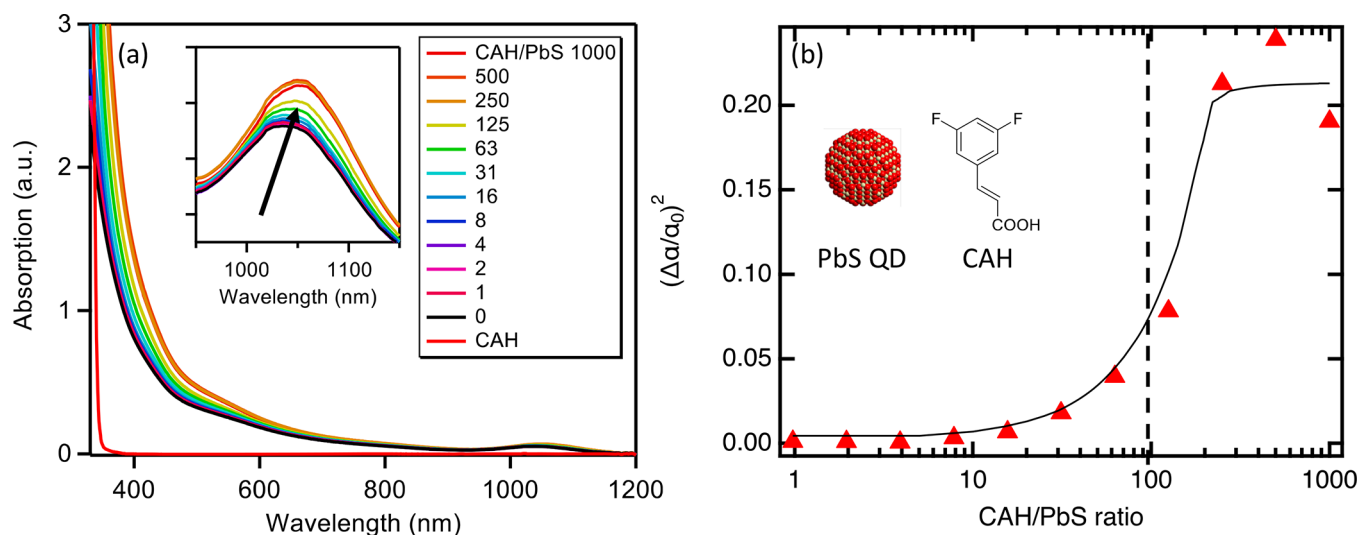


Figure 2. (a) Absorption spectra of PbS QDs, originally terminated with oleic acid (OA), after ligand exchange with 3,5-difluorocinnamic acid (CAH) with different CAH/PbS mole ratios. (inset) Zoom-in on the first exciton peak of PbS QDs. (b) Enhancement of integrated absorption (400–1200 nm) of PbS QDs vs the ratio of CAH/PbS in ligand exchange. The dashed line denotes a CAH/PbS ratio of 100, which is the condition used for preparing Janus PbS QDs for NMR and pyroelectric measurements.

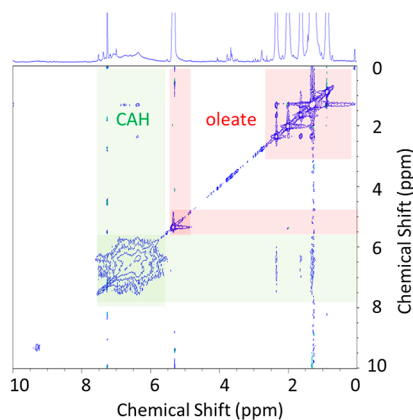


Figure 3. 2D nuclear Overhauser effect spectroscopy (NOESY) of PbS QDs with 3,5-difluorocinnamic acid/OA Janus-ligand shell. The ligand exchange condition follows the one in Figure 1b with the CAH/PbS ratio of 100, which corresponds to 35% coverage of CAH.

ligand shell. The lack of significant cross-peaks suggests the formation of segregated ligand patches,^{18,22,23} as the CAH and OA bound molecules are only next to one another at the boundary of the patches and exhibit a small NOE effect. As shown in Figure 3, the bound CAH ligands show a broad peak in the aromatic region from 5.5 to 8 ppm, and peaks in the aliphatic region reflect the oleic acid ligands. Cross-peaks are barely observed, which indicates the formation of Janus (or patchy) ligand shells. In contrast, strong cross-peaks are observed on PbS QDs ligand exchanged with *p*-cyanocinnamic acid (Figure S2 SI) where the absorption isotherm does not indicate large ligand–ligand cooperativity. This observation contrasts with a recent conclusion¹⁸ that *p*-cyanocinnamic acid should yield a Janus-ligand shell, which could be due to the different sizes of PbS QDs used in this work (3.5 nm) and the prior study (3.2 nm).

Pyroelectric Effect. We demonstrate the pyroelectric effect using two configurations. In the first configuration a matrix-free pyroelectric thin film is prepared by self-assembly of the PbS

QDs with Janus ligand shells under an applied electric field using a customized gold electrode configuration on a Si wafer. PbS QDs after ligand exchange with CAH were washed with acetone as the antisolvent and redispersed in toluene before use. Two 50 nm thick gold electrodes were deposited with 10 μm separation on a semi-insulating silicon wafer (Figure 4).

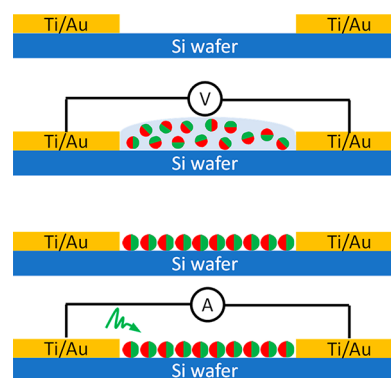


Figure 4. Construction of pyroelectric films of Janus PbS QDs under electric field. The pyroelectric QD solution is dropped in between gold electrodes on Si substrates. QDs are self-assembled under electric fields during the evaporation of solvent (toluene). The pyroelectric current is measured under the illumination of a 532 nm laser.

The Janus PbS QD solution was drop-casted on the channel between the two electrodes. The spontaneous dipole moment of Janus PbS QDs allows them to be aligned with the electric field direction. As toluene dries out, close-packed head-to-tail structures form with the self-assembled QD film (Figure 4), with the ensemble dipole moment pointing from one electrode to the other. The pyroelectric effect of the device is tested by shining a 5 mW 532 nm CW laser on the film and monitoring the current. Absorption of light generates charge carriers, and cooling, and nonradiative recombination of those carriers generates heat, triggering rotation and movement of the QDs. The ordered QDs thus randomly rearrange and the ensemble polarization changes, which modulates the net charge

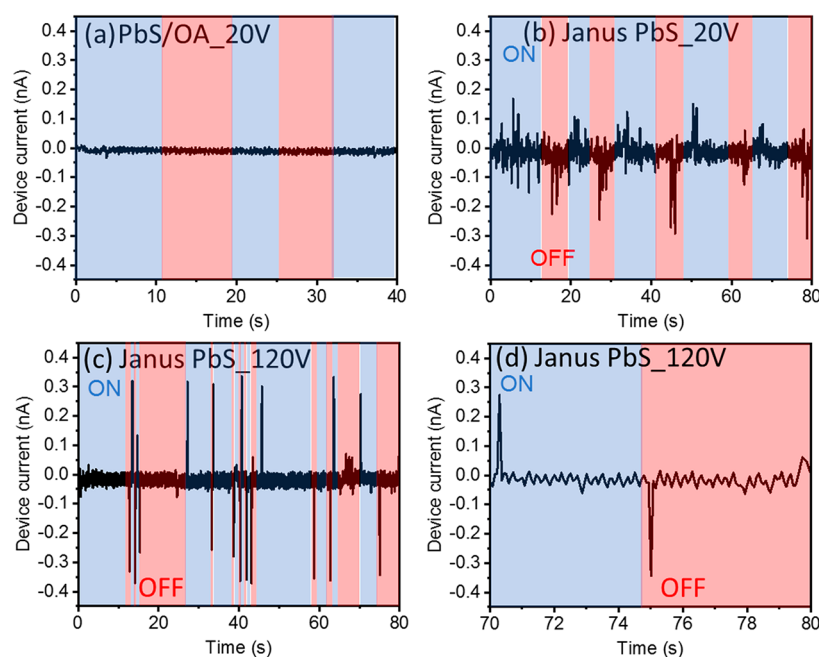


Figure 5. Current response from pyroelectric Janus PbS thin films triggered by the illumination of 5 mW 532 nm laser. The pulse-like current was generated at the moment the laser was turned on or off. (a) PbS/OA QDs assembled under 20 V. (b) Janus PbS QDs assembled under 20 V and (c) 120 V. (d) Zoom-in on the time scale of panel c. For clarity, turning the laser on and off are indicated as blue and red, respectively.

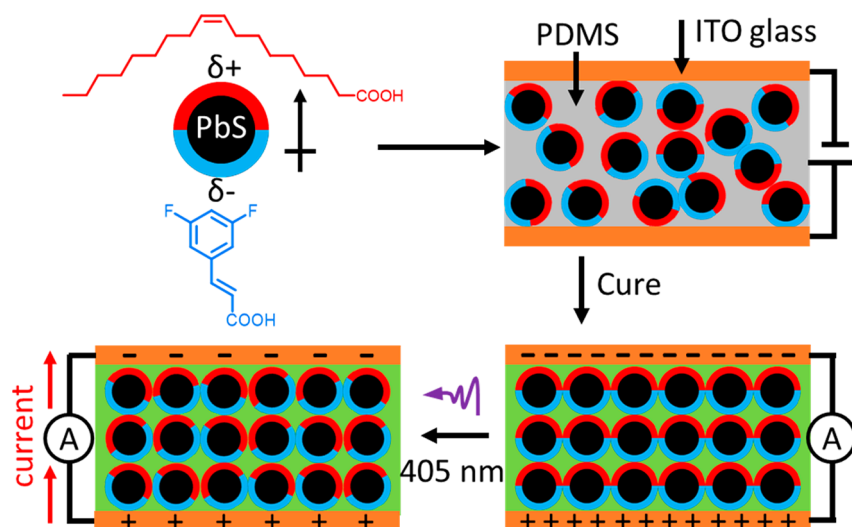


Figure 6. PbS QDs with Janus-ligand shells are premixed with polydimethylsiloxane (PDMS), and the mixture was sandwiched between two pieces of ITO glasses. Films are cured under electric field, and pyroelectric effect is measured with the excitation of 405 nm laser.

distribution at the two ends of the film. The spontaneous change in net charge induces a pyroelectric current under the short circuit condition (Figure 5).

For the device prepared with Janus PbS QDs self-assembled under 20 V (Figure 5b), because the film is only 50 nm thick, and the channel length is tens of micrometers, the heating and cooling process is fast, generating a narrow pulse-like current spike (Figure 5b and c). The pyroelectric current observed here is distinguished from any photocurrent which should be observed as a continuous signal but not a pulse.

The pyroelectric effect of the Janus QD thin film was enhanced when the QD arrays were assembled under a stronger electric field. Figure 5c presents the pyroelectric current generated from the Janus QD film assembled under

120 V. Compared with the results in Figure 5b in which QDs are self-assembled under 20 V, the pyroelectric current is ~ 3 times stronger. This is because the alignment of Janus QDs is dependent on the intensity of the electric field. The stronger voltage allows each QD to be better aligned with the electric field, which yields stronger spontaneous polarization. Therefore, the change of polarization when heated or cooled is more prominent, resulting in a larger pyroelectric effect.

In the second demonstration, the PbS Janus QDs are dispersed into polydimethylsiloxane (PDMS) and premixed colloidal dispersion is applied between two ITO coated glass substrates (Figure 6). QDs are self-assembled in the matrix of PDMS by curing at 60 °C for 2 h while applying a voltage of 150 V. A 5 mW 405 nm CW laser is used to induce a rapid

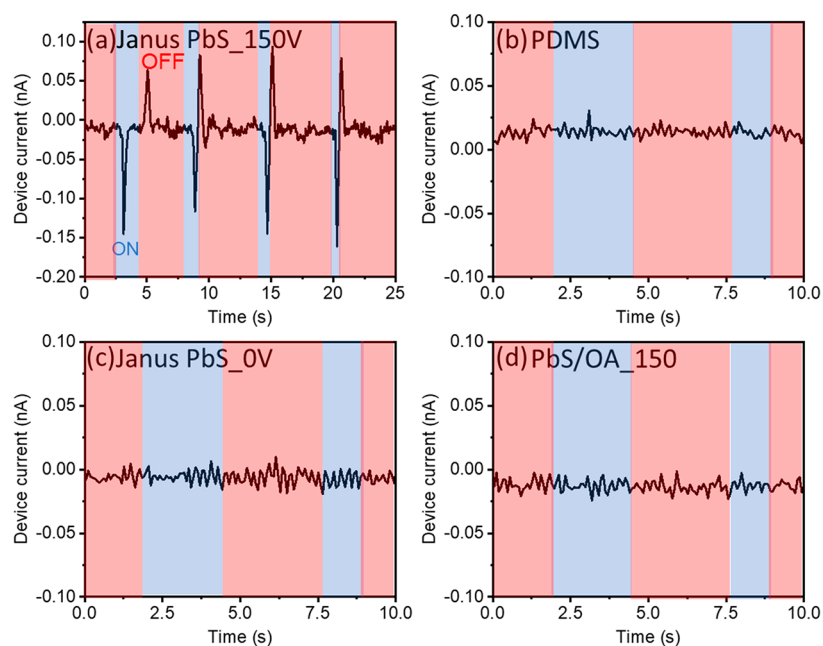


Figure 7. Pyroelectric measurement on devices in Figure 6 under the illumination of 405 nm laser in different conditions: (a) Janus PbS QDs assembled under 150 V; (b) PDMS matrix only; (c) Janus PbS QDs assembled under 0 V; (d). As-synthesized oleic acid capped PbS QDs assembled under 150 V. Blue and red indicate that the 405 nm laser is switched on and off, respectively.

temperature fluctuation within the QD/polymer film. In this architecture, the film thickness is 75 μm which is controlled by the Kapton tape that serves as a spacer between ITO glass substrates, with the fill factor of 0.216. The pyroelectric effect is observed for structures with Janus PbS QDs in the PDMS matrix between ITO glass substrates. As shown in Figure 7a, the pulse-like pyroelectric current is observed when switching the 405 nm laser on and off. We prepared three control films under identical conditions, PDMS without QDs added (Figure 7b), PDMS with Janus-QDs but with no applied field (Figure 7c), and PDMS with QDs that do not have a Janus shell (Figure 7d). Only the sample with Janus-ligand shells that had been fabricated under an applied field shows a current response. This result can only occur if the ligand exchange process produces NCs with an asymmetric ligand shell, thus validating the 2D lattice modeling and 2D NMR experiments discussed above.

The pyroelectric current is proportional to the rate of temperature change, i.e., $I_p = \alpha A(dT/dt)$, where A is the area, α is the pyroelectric coefficient, and dT/dt is the rate of temperature change. A current is only observed while the temperature rapidly changes. Accordingly, when the laser was turned on/off, a positive/negative current pulse was observed. The pulse-like signal was generated only at the moment the laser is turned on/off because the temperature of the film rapidly changes upon absorbing light. With continuous illumination the temperature reaches a steady state for which no pyroelectric current is generated. Similarly, when the light is turned off the film rapidly cools down and generates the opposite current pulse. Thus, the temperature fluctuation triggers the change of the spontaneous polarization within the film, which generates the pyroelectric current. The current only responds to temperature fluctuations and not from the presence or absence of photocarriers.

For pyroelectric films on a thermally conductive substrate, Lubomirsky and Stafsudd have summarized methods to measure pyroelectric coefficients in thin films.²⁴ Specifically,

the heat diffusion equation describes the temperature fluctuation $\partial T/\partial t$ in a particular material over time with the consideration of thermal diffusivity (thermal conductivity divided by volumetric heat capacity) and the rate of heat input. Derived from heat diffusion equation, for step-like heating on a semi-infinite, nonpyroelectric substrate with thermal conductivity, the temperature at the surface of the substrate follows:²⁵

$$T(t) - T_0 = \frac{2q}{\lambda_s} \sqrt{\frac{\lambda_s t}{C_s \pi}} \quad (1)$$

and the pyroelectric current is given by

$$I(t) = \frac{A\alpha q}{\sqrt{\pi\lambda_s C_s t}} \quad (2)$$

where λ_s is the thermal conductivity, which is 0.15 W/m·K²⁶ for the PDMS matrix; and C_s is the thermal capacitance per unit volume, which is 1.63 J/gK;²⁷ for PbS; A is the area of electric contact, which is $2.15 \times 10^{-4} \text{ m}^2$; q is the heat flux, 197.45 W/m² for 405 nm laser; and α is the pyroelectric coefficient. As $I(t)^2$ has been experimentally observed to be linearly correlated with $1/t$,²⁵ the slope of the plot of $I(t)^2$ vs $1/t$ (Figure S3) can be used to obtain the pyroelectric coefficient from eq 2. With all parameters inserted in eq 2, pyroelectric coefficient is calculated as $2.07 \times 10^{-15} \text{ C/m}^2\cdot\text{K}$.

For the first pyroelectric demonstration, the pyroelectric coefficient is calculated to be $1.97 \times 10^{-7} \text{ C/m}^2\cdot\text{K}$; however, this represents a lower limit since the pyroelectric current pulse was faster than our time resolution. Compared to the PDMS matrix, the pyroelectric coefficient is enhanced by at least 8 orders of magnitude. Though this value is still lower than many inorganic crystalline pyroelectric materials,⁵ it is higher than some reported pyroelectric coefficient for polymeric materials by orders of magnitude.²⁸ Additionally, optimizations could be done to improve the performance of Janus QDs as pyroelectric materials. For example, ligand shells with strong electron-

donating/withdrawing effects might be applied to enhance the intrinsic dipole moment of Janus QDs. QDs with Janus inorganic core could also be an alternative for pyroelectric applications. The role of size, shape, or composition will also be explored in the future.

CONCLUSIONS

We demonstrate the ability to construct Janus-ligand shells on QDs and thus control the asymmetry of otherwise spherical semiconductor nanocrystals through the observation of the pyroelectric effect. Asymmetry is an essential property of any functional system. Janus nanoparticles are receiving considerable attention for a wide range of potential applications, ranging from catalysis and biosensing to drug delivery.^{29–31} Here we demonstrate that Janus-ligand shells can be used to fabricate functional QD films and solids. We have observed the pyroelectric effect on two different configurations, with pyroelectric coefficient calculated to be 1.97×10^{-7} and 2.07×10^{-15} C/m²·K, respectively. This work shines light on the design principles of pyroelectric materials, which could be useful for the development of energy harvesting systems.^{32,33}

MATERIALS AND METHODS

Materials. Lead nitrate (99.999%), oleic acid (tech. grade, 90%), 1-octene (98%), phenyl isothiocyanate (98%), aniline (99.5%), trans-3,5-difluorocinnamic acid (99%), and anhydrous solvents of methanol (99.8%), toluene (99.8%), dichloromethane (99.8%), acetonitrile (99.8%), methyl acetate (99.5%), and polydimethylsiloxane (PDMS) were purchased from Sigma-Aldrich. Sodium hydroxide (certified ACS) and anhydrous isopropanol (99.5%) were purchased from Fisher. Bio-Beads for gel permeation chromatography were purchased from Bio-Rad and soaked in dichloromethane overnight. (100)-Oriented, boron-doped silicon (Si) wafers (resistivity = 0.005–0.01 in. cm, thickness = 525 ± 25 nm) with 300 nm of thermal oxide (SiO₂) were purchased from Addison.

PbS QD Synthesis and Purification. PbS QDs were synthesized according to the work of Hendricks et al.³⁴ Lead oleate³⁴ (2.203 g, 2.86 mmol, 1.5 equiv) and 1-octene (36.9 mL) were added to 100 mL 3-necked round-bottom flask in nitrogen glovebox. The solution was then brought out to Schlenk line and stirred at 95 °C for 15 min. *N,N'*-Diphenylthiourea³⁴ (0.436g, 1.91 mmol) and diglyme (1.25 mL) were preheated to 95 °C and injected to lead oleate solution with vigorous stirring. After 60 s, the heating mantle was removed and the reaction was cooled to room temperature. Volatiles were removed under vacuum, and the flask was brought into the glovebox. The cycle of redispersion with toluene (40 mL) and precipitation with methyl acetate (120 mL) was performed 6 times to wash QDs. PbS QDs were finally dissolved in toluene, and stored in the dark in a glovebox.

QD Characterization. *UV–Vis–NIR Absorbance.* Absorption spectra were collected using a Cary 7000 spectrometer.

Transmission Electron Microscopy. TEM images were obtained on an FEI ST30 at 300 kV. TEM samples were prepared by drop-casting a dilute solution of PbS QDs in toluene onto the carbon-coated copper grids.

Ligand Exchange of PbS QDs with Cinnamic Acid. In a nitrogen-filled glovebox, PbS QDs diluted with dichloromethane (6.67 μM) were mixed with a specific amount of cinnamic acid dissolved in solvents. Methyl acetate was used for trans-3,5-difluorocinnamic acid and acetonitrile/isopropanol mixture (v/v = 5:1) was used for trans-4-cyanocinnamic acid. The ligand exchange solution was vigorously stirred for 10 min. For the adsorption isotherm, the solution after ligand exchange was used without further purification. and the molar ratio of cinnamic acid against PbS QDs was adjusted by varying the concentration of an added cinnamic acid solution with the volume of cinnamic acid solution fixed. For NMR and pyroelectric device fabrication, PbS QDs after ligand exchange were purified by gel permeation chromatography with eluent of

dichloromethane. Dichloromethane was removed under vacuum, and PbS QDs were redispersed in toluene for device fabrication and deuterated chloroform for NMR.

Device Fabrication and Pyroelectric Measurement. *Device on SiO₂/Si Substrate.* Two-terminal devices were fabricated by using standard semiconductor fabrication techniques in the cleanroom. The device was patterned by photolithography and 5 nmTi/30 nm Au electrodes were deposited by using the thermal evaporator. Pyroelectric devices were prepared by drop-casting a solution of PbS QDs with Janus ligand shell on the channel while the bias voltage was applied on Ti/Au electrodes through a Keithley 2400 source meter and probe station. Three iterations of drop-casting were performed to make sure QDs are closely packed between electrodes. Pyroelectricity was triggered by a 5 mW 532 nm laser diode and the pyroelectric signal was recorded on Keithley 2400 sourcemeter with a control program with the bias of 1 V continuously applied.³⁵

Device with ITO Glasses. The solution of PbS QDs with Janus ligand shell was concentrated to 3 mM and mixed with an equal volume of PDMS (premixed with curing agent). The mixture was degassed for 1 min and then applied to the space between two pieces of ITO glass. Kapton tape is used as a spacer to control the PDMS film thickness to be 75 μm. The PDMS film was cured at 70 °C for 3 h. Meanwhile, a voltage of 150 V was applied on the two pieces of ITO glasses by Keithley 2400 source meter. Pyroelectricity was triggered by 5 mW 405 nm laser diode and the pyroelectric current was recorded on Keithley 2400 source meter.

ASSOCIATED CONTENT

Supporting Information

The Supporting Information is available free of charge at <https://pubs.acs.org/doi/10.1021/acsnano.1c05185>.

Electronic absorption spectrum, TEM image, 2D NMR spectrum of PbS QDs with *p*-cyanocinnamic acid/OA isotropic ligand shell, plot of the square of pyroelectric current vs inverse time, and detailed fabrication of the PDMS based electronic device (PDF)

AUTHOR INFORMATION

Corresponding Author

Matthew C. Beard – Chemistry & Nanoscience Center, National Renewable Energy Laboratory, Golden, Colorado 80401, United States; orcid.org/0000-0002-2711-1355; Email: matt.beard@nrel.gov

Authors

Zhiyuan Huang – Chemistry & Nanoscience Center, National Renewable Energy Laboratory, Golden, Colorado 80401, United States; orcid.org/0000-0003-4180-0234

Ji Hao – Chemistry & Nanoscience Center, National Renewable Energy Laboratory, Golden, Colorado 80401, United States

Jeffrey L. Blackburn – Chemistry & Nanoscience Center, National Renewable Energy Laboratory, Golden, Colorado 80401, United States; orcid.org/0000-0002-9237-5891

Complete contact information is available at: <https://pubs.acs.org/10.1021/acsnano.1c05185>

Notes

The authors declare no competing financial interest.

ACKNOWLEDGMENTS

This work was authored in part by the National Renewable Energy Laboratory (NREL), operated by Alliance for Sustainable Energy LLC, for the U.S. Department of Energy (DOE) under contract no. DE-AC36-08GO28308. Funding

provided by BES Solar Photochemistry Program funded by the Office of Basic Energy Sciences, Office of Science within the US Department of Energy through contract number DE-AC36-08GO28308 with NREL. The views expressed in this article do not necessarily represent the views of the DOE or the U.S. Government.

REFERENCES

- (1) Lawrence Livermore National Laboratory. Estimated Energy Use in 2020:92.9 Quads. <https://flowcharts.llnl.gov/> (accessed 2021).
- (2) DiSalvo, F. J. Thermoelectric Cooling and Power Generation. *Science* **1999**, *285* (5428), 703–706.
- (3) Bell, L. E. Cooling, Heating, Generating Power, and Recovering Waste Heat with Thermoelectric Systems. *Science* **2008**, *321* (5895), 1457–1461.
- (4) Khodayari, A.; Mohammadi, S.; Guyomar, D. *Pyroelectric Energy Harvesting: Fundamentals and Applications*, 1st ed.; VDM Publishing: Riga, 2011; Vol. 1, pp 1–128.
- (5) Bowen, C. R.; Taylor, J.; LeBoulbar, E.; Zabek, D.; Chauhan, A.; Vaish, R. Pyroelectric Materials and Devices for Energy Harvesting Applications. *Energy Environ. Sci.* **2014**, *7* (12), 3836–3856.
- (6) Lang, S. B.; Das-Gupta, D. K., Chapter 1—Pyroelectricity: Fundamentals and Applications. In *Handbook of Advanced Electronic and Photonic Materials and Devices*; Singh Nalwa, H., Ed.; Academic Press: Burlington, 2001; pp 1–55.
- (7) Lingam, D.; Parikh, A. R.; Huang, J.; Jain, A.; Minary-Jolandan, M. Nano/Microscale Pyroelectric Energy Harvesting: Challenges and Opportunities. *Int. J. Smart Nano Mater.* **2013**, *4* (4), 229–245.
- (8) Yu, P.; Tang, Y.; Luo, H. Fabrication, Property and Application of Novel Pyroelectric Single Crystals—PMN—PT. *J. Electroceram.* **2010**, *24* (1), 1–4.
- (9) Lukasiewicz, T.; Swirkowicz, M. A.; Dec, J.; Hofman, W.; Szyrski, W. Strontium–Barium Niobate Single Crystals, Growth and Ferroelectric Properties. *J. Cryst. Growth* **2008**, *310* (7), 1464–1469.
- (10) Bowen, C. R.; Kim, H. A.; Weaver, P. M.; Dunn, S. Piezoelectric and Ferroelectric Materials and Structures for Energy Harvesting Applications. *Energy Environ. Sci.* **2014**, *7* (1), 25–44.
- (11) Ozgur, U.; Gu, X.; Chevtchenko, S.; Spradlin, J.; Cho, S. J.; Morkoc, H.; Pollak, F. H.; Everitt, H. O.; Nemeth, B.; Nause, J. E. Thermal Conductivity of Bulk ZnO after Different Thermal Treatments. *J. Electron. Mater.* **2006**, *35* (4), 550–555.
- (12) Park, T.; Na, J.; Kim, B.; Kim, Y.; Shin, H.; Kim, E. Photothermally Activated Pyroelectric Polymer Films for Harvesting of Solar Heat with a Hybrid Energy Cell Structure. *ACS Nano* **2015**, *9* (12), 11830–11839.
- (13) Whatmore, R. W. Pyroelectric Devices and Materials. *Rep. Prog. Phys.* **1986**, *49* (12), 1335–1386.
- (14) Lang, S. B. Pyroelectricity: From Ancient Curiosity to Modern Imaging Tool. *Phys. Today* **2005**, *58* (8), 31–36.
- (15) Alam, M. M.; Sultana, A.; Mandal, D. Biomechanical and Acoustic Energy Harvesting from TiO₂ Nanoparticle Modulated PVDF Nanofiber Made High Performance Nanogenerator. *ACS Applied Energy Materials* **2018**, *1* (7), 3103–3112.
- (16) Martins, P.; Lopes, A. C.; Lanceros-Mendez, S. Electroactive Phases of Poly(vinylidene Fluoride): Determination, Processing and Applications. *Prog. Polym. Sci.* **2014**, *39* (4), 683–706.
- (17) Fortunato, M.; Cavallini, D.; De Bellis, G.; Marra, F.; Tamburrano, A.; Sarto, F.; Sarto, M. S. Phase Inversion in PVDF Films with Enhanced Piezoresponse through Spin-Coating and Quenching. *Polymers* **2019**, *11* (7), 1096.
- (18) Bronstein, N. D.; Martinez, M. S.; Kroupa, D. M.; Vörös, M.; Lu, H.; Brawand, N. P.; Nozik, A. J.; Sellinger, A.; Galli, G.; Beard, M. C. Designing Janus Ligand Shells on PbS Quantum Dots Using Ligand–Ligand Cooperativity. *ACS Nano* **2019**, *13* (4), 3839–3846.
- (19) Giansante, C.; Infante, I.; Fabiano, E.; Grisorio, R.; Suranna, G. P.; Gigli, G. Darker-Than-Black” PbS Quantum Dots: Enhancing Optical Absorption of Colloidal Semiconductor Nanocrystals via Short Conjugated Ligands. *J. Am. Chem. Soc.* **2015**, *137* (5), 1875–1886.
- (20) Giansante, C.; Carbone, L.; Giannini, C.; Altamura, D.; Ameer, Z.; Maruccio, G.; Loiudice, A.; Belviso, M. R.; Cozzoli, P. D.; Rizzo, A.; Gigli, G. Colloidal Arenethiolate-Capped PbS Quantum Dots: Optoelectronic Properties, Self-Assembly, and Application in Solution-Cast Photovoltaics. *J. Phys. Chem. C* **2013**, *117* (25), 13305–13317.
- (21) Kroupa, D. M.; Anderson, N. C.; Castaneda, C. V.; Nozik, A. J.; Beard, M. C. In Situ Spectroscopic Characterization of a Solution-Phase X-Type Ligand Exchange at Colloidal Lead Sulphide Quantum Dot Surfaces. *Chem. Commun.* **2016**, *52* (96), 13893–13896.
- (22) Ong, Q.; Luo, Z.; Stellacci, F. Characterization of Ligand Shell for Mixed-Ligand Coated Gold Nanoparticles. *Acc. Chem. Res.* **2017**, *50* (8), 1911–1919.
- (23) Walther, A.; Muller, A. H. E. Janus Particles: Synthesis, Self-Assembly, Physical Properties, and Applications. *Chem. Rev.* **2013**, *113* (7), 5194–5261.
- (24) Lubomirsky, I.; Stafsudd, O. Invited Review Article: Practical Guide for Pyroelectric Measurements. *Rev. Sci. Instrum.* **2012**, *83* (5), 051101.
- (25) Ehre, D.; Lyahovitskaya, V.; Tagantsev, A.; Lubomirsky, I. Amorphous Piezo- and Pyroelectric Phases of BaZrO₃ and SrTiO₃. *Adv. Mater.* **2007**, *19* (11), 1515–1517.
- (26) Mark, J. E. *Polymer Data Handbook*, 2nd ed.; Oxford University Press: New York, 2009; Vol. 1, pp 424.
- (27) Zhang, G.; Sun, Y.; Qian, B.; Gao, H.; Zuo, D. Experimental Study on Mechanical Performance of Polydimethylsiloxane (PDMS) at Various Temperatures. *Polym. Test.* **2020**, *90*, 106670.
- (28) Sultana, A.; Ghosh, S. K.; Alam, M. M.; Sadhukhan, P.; Roy, K.; Xie, M.; Bowen, C. R.; Sarkar, S.; Das, S.; Midya, T. R.; Mandal, D. Methylammonium Lead Iodide Incorporated Poly(vinylidene Fluoride) Nanofibers for Flexible Piezoelectric–Pyroelectric Nanogenerator. *ACS Appl. Mater. Interfaces* **2019**, *11* (30), 27279–27287.
- (29) Kirillova, A.; Marschelke, C.; Synytska, A. Hybrid Janus Particles: Challenges and Opportunities for the Design of Active Functional Interfaces and Surfaces. *ACS Appl. Mater. Interfaces* **2019**, *11* (10), 9643–9671.
- (30) Su, H.; Hurd Price, C. A.; Jing, L.; Tian, Q.; Liu, J.; Qian, K. Janus Particles: Design, Preparation, and Biomedical Applications. *Materials Today Bio* **2019**, *4*, 100033.
- (31) Zhang, X.; Fu, Q.; Duan, H.; Song, J.; Yang, H. Janus Nanoparticles: From Fabrication to (Bio)Applications. *ACS Nano* **2021**, *15* (4), 6147–6191.
- (32) Yang, Y.; Zhou, Y.; Wu, J. M.; Wang, Z. L. Single Micro/Nanowire Pyroelectric Nanogenerators as Self-Powered Temperature Sensors. *ACS Nano* **2012**, *6* (9), 8456–8461.
- (33) Wang, X.; Dai, Y.; Liu, R.; He, X.; Li, S.; Wang, Z. L. Light-Triggered Pyroelectric Nanogenerator Based on a *pn*-Junction for Self-Powered Near-Infrared Photosensing. *ACS Nano* **2017**, *11* (8), 8339–8345.
- (34) Hendricks, M. P.; Campos, M. P.; Cleveland, G. T.; Jen-La Plante, I.; Owen, J. S. A Tunable Library of Substituted Thiourea Precursors to Metal Sulfide Nanocrystals. *Science* **2015**, *348* (6240), 1226–1230.
- (35) Wang, Z.; Yu, R.; Pan, C.; Li, Z.; Yang, J.; Yi, F.; Wang, Z. L. Light-Induced Pyroelectric Effect as an Effective Approach for Ultrafast Ultraviolet Nanosensing. *Nat. Commun.* **2015**, *6* (1), 8401.